3. RESULTS

3.1 Inactivation of $K_{Ca}3.1$ gene

3.1.1 Generation of the $K_{Ca}3.1$ knockout mouse

For the generation of $K_{Ca}3.1^{-/-}$ mice two different gene targeting strategies were employed: The first strategy was the conventional strategy (see introduction part for details), the second was the conditional gene targeting strategy initiated at the same time in case embryonic lethality occurs using the first strategy, thus, insuring the analysis of gene function in adult animals.

The targeting vectors pTV5 and P4 were constructed in details as described in the method part. In short, pTV5 vector contains a positive drug selection cassette between two homology arms and another negative selection cassette downstream of homology arm. In P4 vector, *loxP* sites were introduced upstream and downstream of the exon 4 of the $K_{Ca}3.1$ gene. A third *loxP* site flanked a cassette allowing positive and negative drug selection that was inserted downstream of exon 4. All three *loxP* sites were placed in head-to-tail orientation (Figure 3.1). Both DNA sequencing results of pTV5 and P4 vectors showed 100% identity with the published sequence.

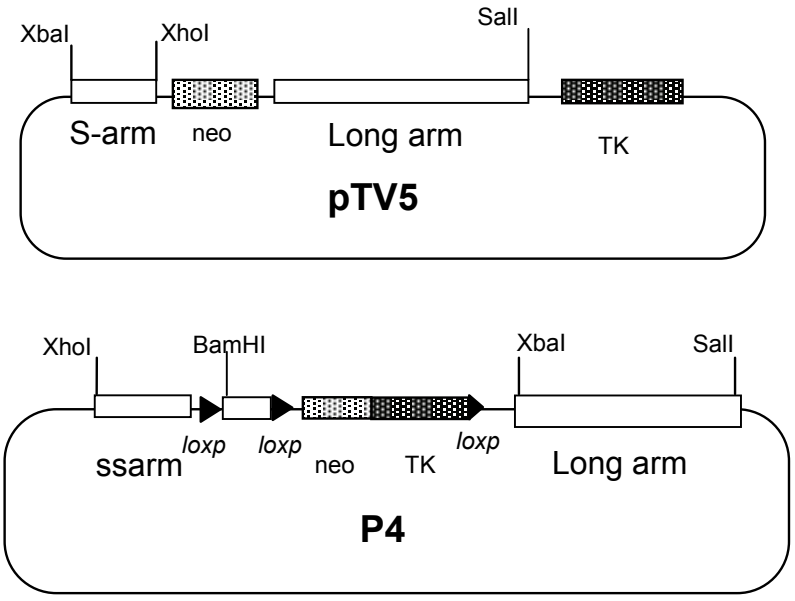

Figure 3.1 Targeting constructs pTV5 and P4 for homologous recombination. pTV5 is used for the complete gene targeting experiment, while P4, using 3-*loxp* system is primarily employed for the conditional gene targeting experiment. White bars indicate the homologous DNA fragments of the $K_{Ca}3.1$ gene. The neo, TK genes are shown in hatched bars. The black triangles indicate the positions of the *loxp* sites. The portions of the plasmids represented by the bars are not drawn to scale.

With these vectors in hand, transfection experiments were carried out according to the protocols described in the method part. In theory, positive selection with neomycin serves for the enrichment of P4 transformed colonies, which were subsequently tested for homologous recombination by PCR with an amplicon spanning the exon4 of the targeting vector (Figure 2.2). However, unfortunately, from 998 colonies survived after neomycin selection for 6 days, none of them showed a homologous recombination. Therefore, this vector was kept at -20° C for future study.

From 238 pTV5 transformed ES cell colonies, only one positive colony showed homologous recombination by PCR following neomycin and

gancyclovir double selection.

ES cells expended from the pTV5 targeted positive colony were microinjected into C57Bl/6 blastocysts and reimplanted into pseudo-pregnant foster mice. Chimerisms of the offspring were quite high (about 80%). Three chimeric mice were mated to wild type C57Bl/6 female mice, and brown offspring were screened for the presence of the mutant allele using a PCR assay, and verified with a southern blot analysis. Six pairs of heterozygous mice ($K_{Ca}3.1^{+/-}$) were selected as founders for the breeding of homozygous ($K_{Ca}3.1^{-/-}$) knockout mice.

3.1.2 Genotyping of the K_{Ca}3.1 knockout mice

Offspring from heterozygous breeding pairs were screened by PCR for the presence of the homozygous mutant allele and verified by southern blot analysis. PCR reactions were carried out for routine mouse genotyping with following primers: Kc4, exon4rev and neorev (sequences see method part). Among them Kc4 binds to the intron which lies upstream of the exon4 of K_{Ca}3.1 gene, exon4rev is specific for exon4 and neorev binds to the neo resistant gene (Figure 3.2 A), thus the multiplex PCR yielded 320 bp for the neo resistant gene and 160 bp for the wild type K_{Ca}3.1 allele. The representative PCR result (Figure 3.2 B) shows a 320 bp band in homozygous K_{Ca}3.1 null mice, a 160 bp band in homozygous wild type mice, while two bands in heterozygous mice as they have both the exon4 of K_{Ca}3.1 gene and the neo resistant gene.

The probe (Figure 3.2 A) used in southern analysis is a 1063 bp DNA fragment amplified using primer set longsouthfor and longsouthrev (sequences refer to method part). The probe hybridizes to complementary DNA fragments digested by endonuclease BglII. The blot result shows a 3.3 kb band, a 4.1 kb

band in $K_{Ca}3.1$ wild-type and homozygous knockout mice, respectively, and both bands in heterozygous mice (Figure 3.2 C) due to the inserted neo resistant gene which is 0.8 kb larger than exon4. This southern blot result further confirms that the pTV5 vector has been homologously integrated into the $K_{Ca}3.1$ locus in the mouse genome and, by breeding, knockout mice are homozygous $K_{Ca}3.1$ null.

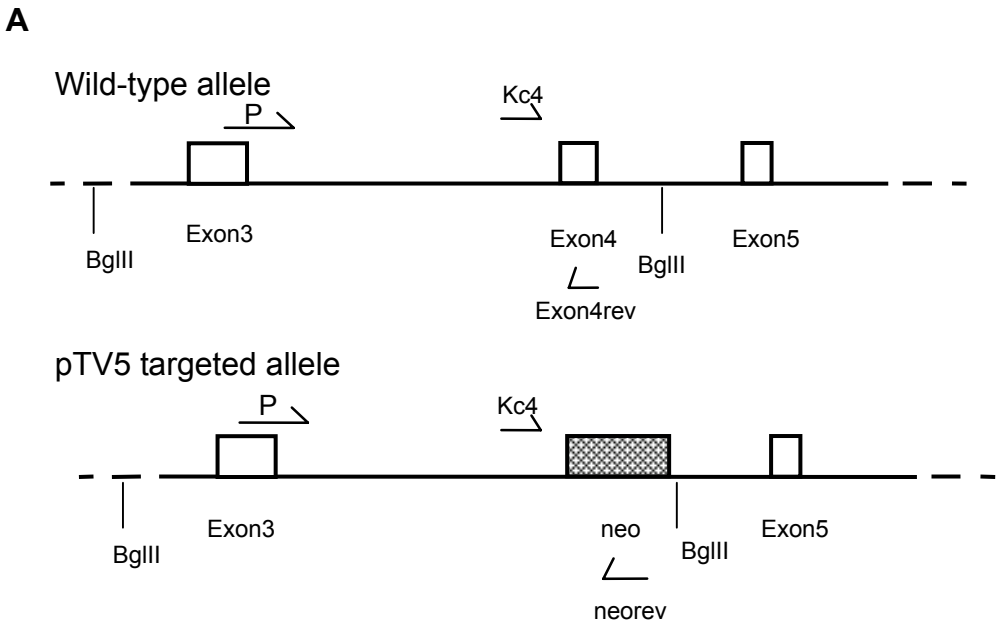

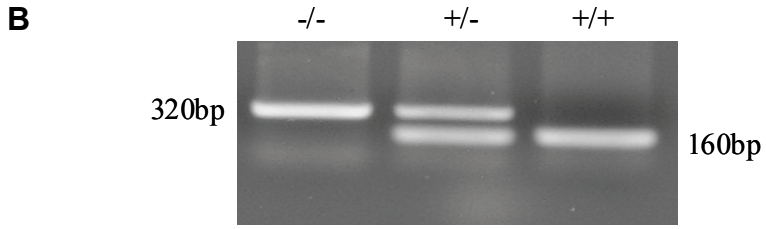

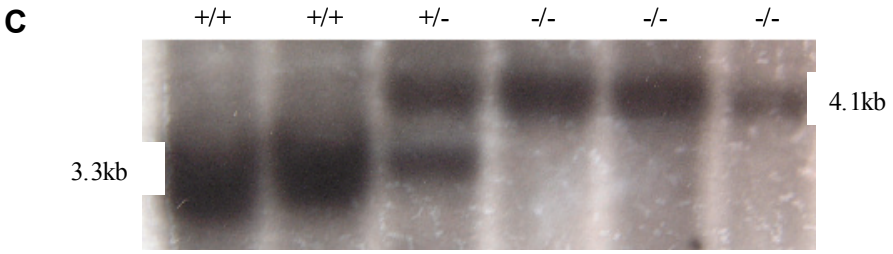

Figure 3.2 PCR and southern blot analysis of mutant mice. **A**. Localization of PCR primers and southern blot probe used for genotyping of the $K_{Ca}3.1$ mutant mice. P stands for the probe of the southern blot. In the pTV5 targeted allele, exon4 has been replaced by the neo resistant gene which is 800 bp larger than exon4. **B**. Routine multiplex PCR for genotyping. **C**. Southern blot analysis for genotyping. +/+, +/- and -/- represents wild-type, heterozygous, and $K_{Ca}3.1$ knockout animal, respectively.

Moreover, mRNAs from mice spleen were used in RT-PCR to investigate the $K_{Ca}3.1$ gene expression in transgenic animals. About 1 µg total RNA extracted from mouse spleen was reverse transcribed followed by PCR using primer sets (sequences refer to method part): fibronestfor, fibronestrev (for the positive control), souprobfor, exon4for, exon5rev (for the negative control, wild-type as well as knockout mice). The result shows that $K_{Ca}3.1$ mRNA was not detectable in knockout mice due to the disruption of mRNA transcription.

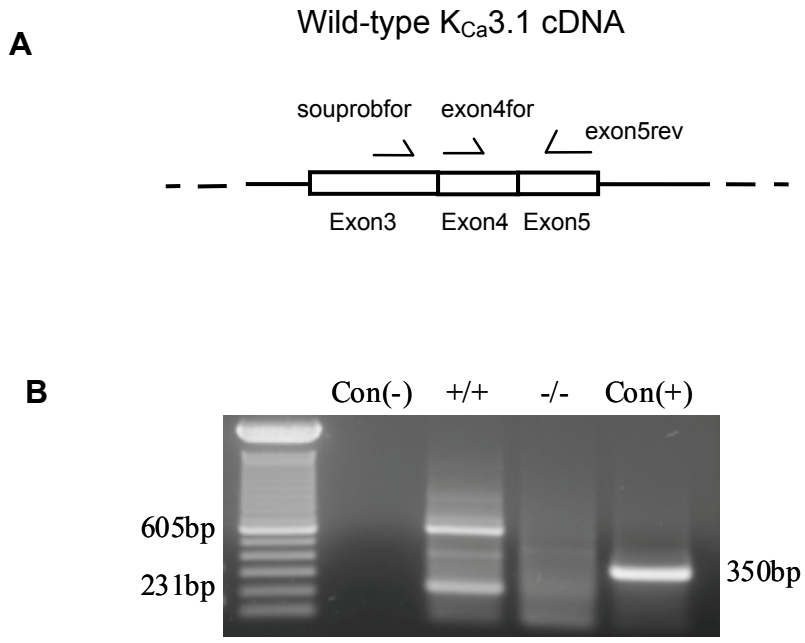

Figure 3.3 RT-PCR analysis of transgenic mice. **A**. Positions of primers used in PCR following reverse transcription. **B**. RT-PCR analysis of $K_{Ca}3.1$ gene expression. Con(-) represents the negative control containing no RNA but just distilled H_2O, while Con(+) stands for positive control (fibronectin gene expression) using knockout mice mRNA as template. +/+, +/- and -/- represents wild-type, heterozygous and $K_{Ca}3.1$ knockout animal, respectively.

Whereas the wild type shows a 605 bp and a 231 bp band as expected from figure 3.3 A. The positive control using mRNA from the knockout is designed to test the quality of the RT product and the result shows a significant band of fibronectin (Figure 3.3 B). The negative control without any mRNA template

but just water shows no band at all. Taken together, $K_{Ca}3.1$ mRNA transcription in $K_{Ca}3.1^{-/-}$ mice is absent resulting from the gene targeting by the pTV5 construct.

In order to demonstrate the absence of the functional $K_{Ca}3.1$ channel expression in $K_{Ca}3.1^{-/-}$ mice, whole-cell patch-clamp experiments were performed using freshly isolated $CD4^+$ T-cells because T-cells are known to express $K_{Ca}3.1$ as the only K_{Ca} channel (Beeton, Wulff *et al.* 2001; Wulff, Calabresi *et al.* 2003). For the identification of K_{Ca} currents, cells were dialyzed with a K^+ pipette solution containing 3 µmol/L $[Ca^{2+}]_i$. To compare the currents between different cells, all measured currents were standardized to cell capacitance. Dialysis of T-cells of wild-type animals with 3 µmol/L Ca^{2+} induced a hyperpolarizing outward current with slightly inward rectification at positive membrane voltages. The reversal potentials extrapolated from the current-voltage relations were around -80 mV and thus near the K^+ equilibrium potential (Figure 3.4 A). This indicates K^+-selectivity of this current as well as Ca^{2+} dependence of K^+ channel activation. To minimize the contamination by any other non-selective currents, K^+ current densities were determined at 0 mV of membrane potential. On the basis of this consideration, $CD4^+$ T-cells from $K_{Ca}3.1^{+/+}$ mice showed an about 154 pA/pF current density at a membrane potential of 0 mV. The Ca^{2+}-activated K^+ current was abolished by the $K_{Ca}3.1$ blocker ChTX (Figure 3.4 A), while $CD4^+$ T-cells from $K_{Ca}3.1^{-/-}$ mice only showed a residual, non-detectable current of about 2 pA/pF at 0 mV (Figure 3.4 B).

These T-cell patch-clamping experiments indicate that ChTX-sensitive $K_{Ca}3.1$ currents are present in $K_{Ca}3.1^{+/+}$ mice but absent in $K_{Ca}3.1^{-/-}$ mice T-cells. In addition, no $K_{Ca}3.1$ current was detectable in freshly isolated ECs of $K_{Ca}3.1^{-/-}$ mice as well, as stated in more detail in following section.

Taken together, the genotyping of the generated mutant mice shows that the $K_{Ca}3.1$ gene expression has been disrupted and subsequently no functional $K_{Ca}3.1$ channel is present in $K_{Ca}3.1^{-/-}$ mice.

A

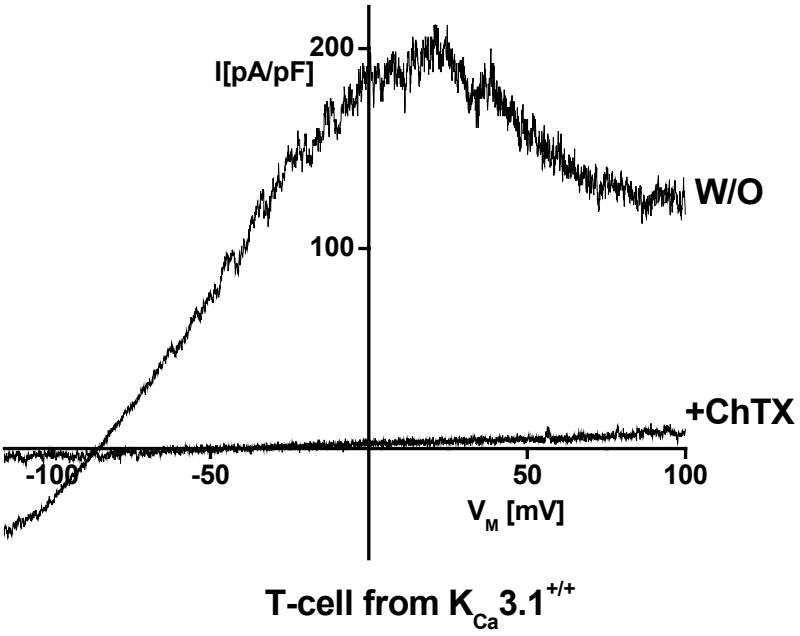

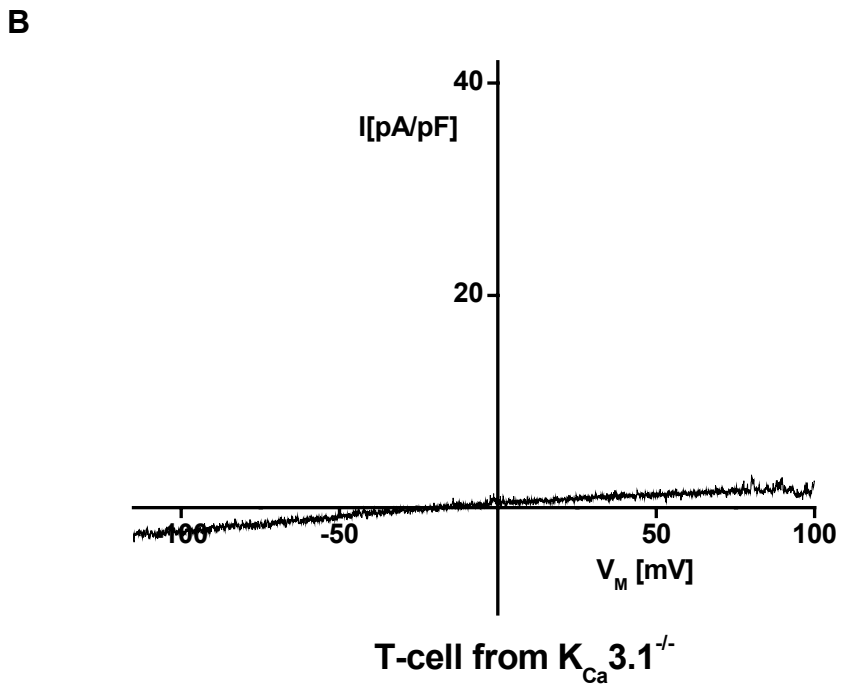

Figure 3.4 Representative current recordings in T-cells from $K_{Ca}3.1^{-/-}$ mice and their wild-type littermates. For K_{Ca} channel activation, cells were dialyzed with a 135 mmol/L K^+ pipette solution containing 3 µmol/L $[Ca^{2+}]_i$. **A**. Whole-cell currents recorded in a T-cell from $K_{Ca}3.1^{+/+}$ mice in the absence (w/o) and presence of 100 nmol/L ChTX. **B**. Whole-cell currents recorded in a T-cell from $K_{Ca}3.1^{-/-}$ mice. Note that T-cell from $K_{Ca}3.1^{-/-}$ mice showed no detectable K_{Ca} current. I indicates current standardized to the cell capacitance; V_m, membrane potential; w/o, without any blocker; Apa, apamin; ChTX, charybdotoxin.

Till present, 571 offspring from heterozygous breeding pairs have been produced and screened. Among them 22.9% are $K_{Ca}3.1^{-/-}$ mice and 24.7% are $K_{Ca}3.1^{+/+}$ mice, rest of them (52.3%) are heterozygous mice. These data are in accordance with the Mendelian law of inheritance. The behavior of all homozygous as well as heterozygous mice was apparently normal and no overt signs of morphological, neuronal, and motoric deficits were detectable. Two interbreeding pairs of homozygous $K_{Ca}3.1$ mutant mice both showed normal size of pups (6-12) in each delivery and backcrossing using male knockout mice and female C57Bl/6 also showed normal fertility. By far $K_{Ca}3.1^{-/-}$ mice stay healthy for 9 months.

3.2 General morphological and histological characteristics of major organs of $K_{Ca}3.1^{-/-}$ mice

Female and male mice were sacrificed at 10 to 18 weeks of age under ether anesthesia by excising the heart and mouse necropsy was carried out to investigate whether or not the absence of $K_{Ca}3.1$ channel caused overt pathological changes in organs or tissue morphology. Body weight of the animal and the weights of major internal organs e.g. heart, liver, spleen, left kidney, right kidney, bladder, and intestine were determined. Organs were subsequently kept in 10% neutral buffered formalin for histology studies.

To compare the organ weight between different mice, all measured organ weights were standardized to body weight. Internal organs examined were heart, liver, spleen, left kidney, right kidney, bladder and intestine and among all animals and from both sexes. These data showed that $K_{Ca}3.1^{-/-}$ mice of both sexes have substantially heavier and larger spleens than their wild-type littermates (Figure 3.5 A, B and D). In female $K_{Ca}3.1^{-/-}$ mice, both heart and left kidney also showed about 10% higher weights than female wild-type mice (Figure 3.5 A). Histological examination revealed no gross pathological changes in spleen as well as in kidney (Figure 3.5 D&E). However, female but not male $K_{Ca}3.1^{-/-}$ mice showed a significant left ventricular hypertrophy (LVH), i.e. the thickening of the left ventricular wall, when compared to female wild-type littermates (Figure 3.5 C).

Taken together, these data indicate that the inactivation of $K_{Ca}3.1$ channel mainly resulted in a significant (up to 1.5-fold) increase of spleen weight and LVH in female mice.

A

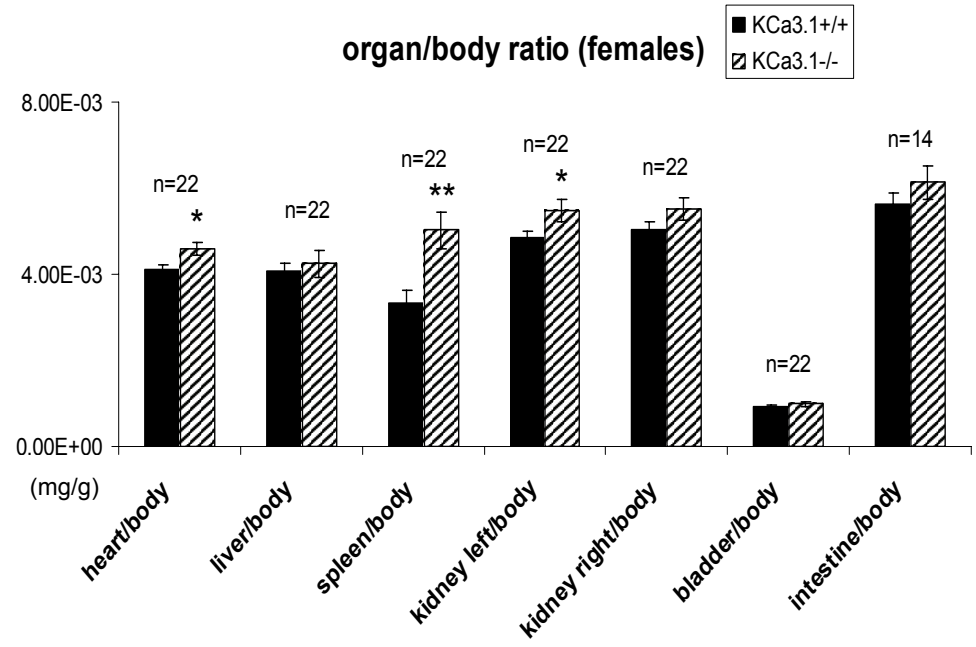
organ/body ratio (females)
KCa3.1+/+
KCa3.1-/-
8.00E-03
4.00E-03
0.00E+00
(mg/g)
n=22
*
n=22
n=22
**
n=22
*
n=22
n=22
n=14
heart/body
liver/body
spleen/body
kidney left/body
kidney right/body
bladder/body
intestine/body

B

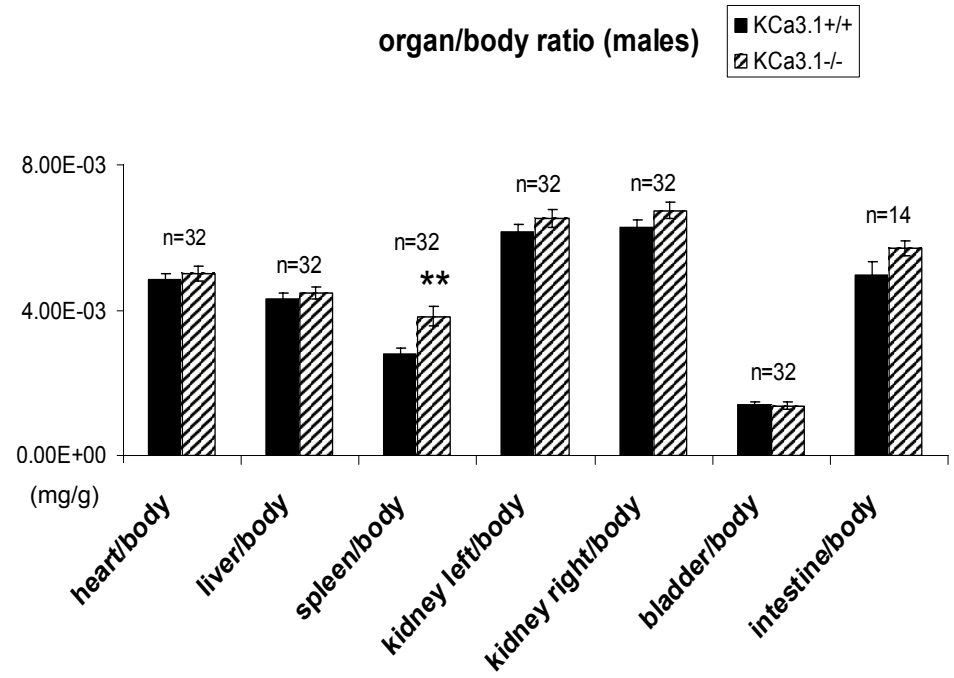
organ/body ratio (males)
KCa3.1+/+
KCa3.1-/-
8.00E-03
4.00E-03
0.00E+00
(mg/g)
n=32
n=32
n=32
**
n=32
n=32
n=32
n=14
heart/body
liver/body
spleen/body
kidney left/body
kidney right/body
bladder/body
intestine/body

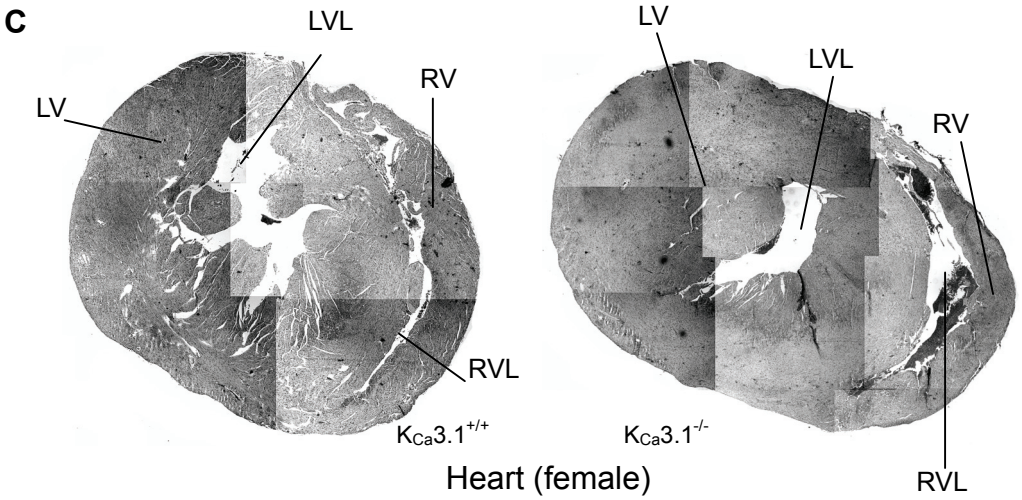
C
LVL
LV
RV
RVL
$K_{Ca}3.1^{+/+}$
LV
LVL
RV
RVL
$K_{Ca}3.1^{-/-}$
Heart (female)

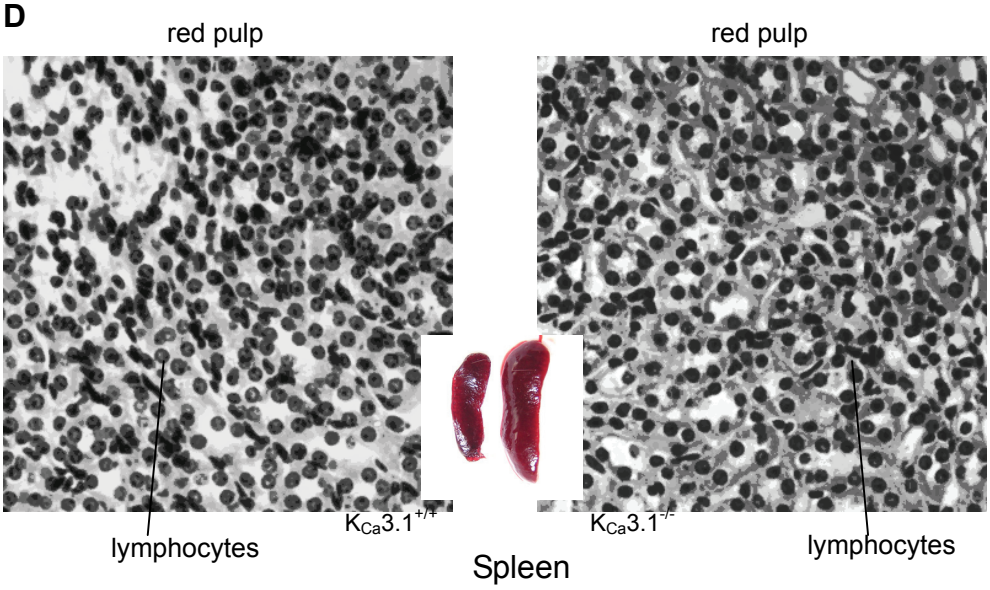
D
red pulp
lymphocytes
$K_{Ca}3.1^{+/+}$
red pulp
$K_{Ca}3.1^{-/-}$
lymphocytes
Spleen

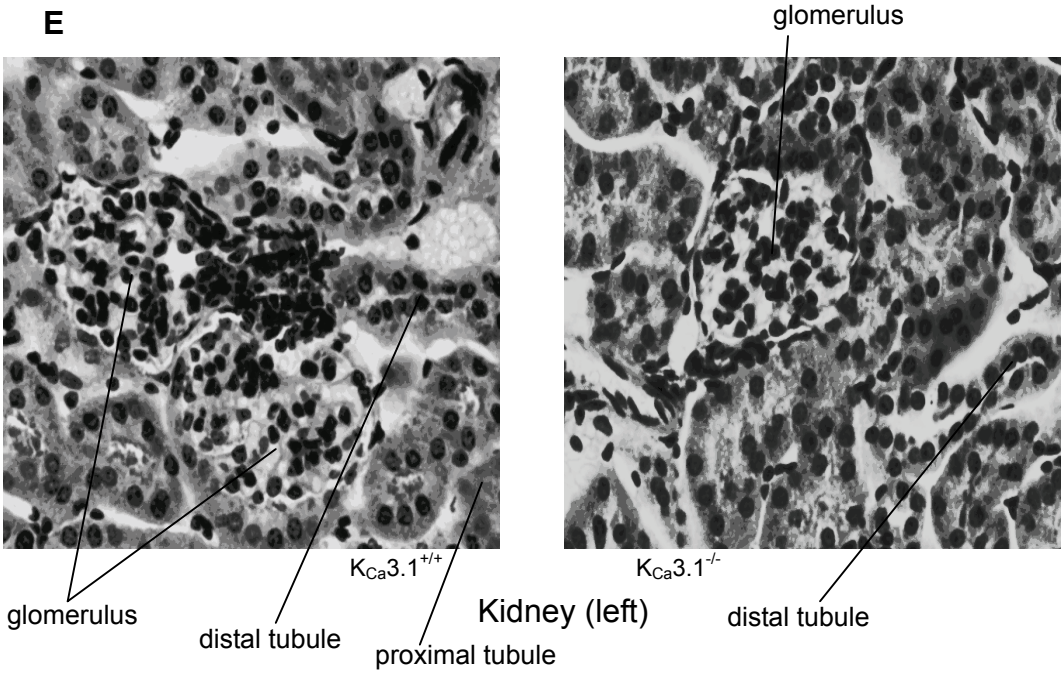
E
glomerulus
distal tubule
proximal tubule
$K_{Ca}3.1^{+/+}$
glomerulus
$K_{Ca}3.1^{-/-}$
distal tubule
Kidney (left)

Figure 3.5 Comparisons of morphological and histological data between $K_{Ca}3.1^{-/-}$ and wild-type mice. Organ weights were standardized to body weight. Internal organs were heart, liver, spleen, left kidney, right kidney, bladder and intestine. **A**. Organ weights of female $K_{Ca}3.1^{-/-}$ and $K_{Ca}3.1^{+/+}$ animals. **B**. Organ weights of male $K_{Ca}3.1^{-/-}$ and $K_{Ca}3.1^{+/+}$ animals. **P*<0.05, ***P*<0.01. Black column stands for $K_{Ca}3.1^{+/+}$ mice, hatched column represents $K_{Ca}3.1^{-/-}$ mice. Values for liver and intestine were divided by 10 and 20 respectively to fit to the chart. **C**. Sections of hearts (left: female wild-type; right, female $K_{Ca}3.1^{-/-}$) showed a significant LVH in $K_{Ca}3.1^{-/-}$ female mice. LV means left ventricle; LVL, left ventricle lumen; RV, right ventricle; RVL, right ventricle lumen. **D**. Sections of red pulps of spleens did not show any obvious pathophysiological changes between $K_{Ca}3.1^{-/-}$ and wild-type mice (left: wild-type; right, $K_{Ca}3.1^{-/-}$). Note that the spleen of $K_{Ca}3.1^{-/-}$ mouse was much bigger than that of $K_{Ca}3.1^{+/+}$ mouse. **E**. Sections of left kidneys did not show any obvious pathophysiological changes between $K_{Ca}3.1^{-/-}$ and wild-type female mice (left: wild-type; right, $K_{Ca}3.1^{-/-}$).

3.3 Characterization of K_{Ca} current

3.3.1 Components of the K_{Ca} current in mice

Whole-cell patch-clamp experiments were performed to investigate K_{Ca} channel currents in both mutant mice and their wild-type counterparts. Freshly isolated mice aortic endothelial cells were used for these experiments. For K_{Ca} channel activation, cells were dialyzed with a 135 mmol/L K^+ pipette solution containing 3 µmol/L $[Ca^{2+}]_i$. Bath solution contained 3 mmol/L K^+. To compare the currents between different cells, all measured currents were standardized to the cell capacitances.

Whole-cell recordings of aortic ECs from $K_{Ca}3.1^{-/-}$ mice and their wild-type littermates showed that dialysis with 3 µmol/L Ca^{2+} induced a hyperpolarizing outward current with slight inward rectification at positive membrane voltages. Representative current traces are shown in Figure 3.6 A, B, C and D. The reversal potentials extrapolated from current-voltage relations were around

-80 mV that is near the K^+ equilibrium potential, thus indicating K^+-selectivity of this Ca^{2+}-activated current. Pharmacological tools were applied during patch-clamp experiments, e.g. the selective $K_{Ca}2.3$ blocker apamin (Apa) and UCL1684 as well as the selective $K_{Ca}3.1$ blocker TRAM-34 and charybdotoxin (ChTX). To clearly characterize $K_{Ca}3.1$ currents, experiments were performed in the presence of the selective $K_{Ca}2.3$ blocker UCL1684 (100 nmol/L). Under such condition, the K_{Ca} currents in ECs of wild-type animals were completely abolished by TRAM-34 (Figure 3.6 A), while no K_{Ca} current was detectable under the same condition in $K_{Ca}3.1^{-/-}$ ECs (Figure 3.6 B). In another set of experiments, which was absent of UCL1684, K_{Ca} currents in aortic ECs of wild-type animals were abolished by the combination of Apa and ChTX (Figure 3.6 C), whereas the K_{Ca} currents in ECs of $K_{Ca}3.1^{-/-}$ mice were abolished solely by Apa (Figure 3.6 D). Thus, these experiments clearly showed that $K_{Ca}3.1$ current was present in wild-type ECs but absent in ECs of $K_{Ca}3.1^{-/-}$ mice.

Statistically, the total K_{Ca} current densities determined at 0 mV of membrane potential were significantly less in female $K_{Ca}3.1^{-/-}$ mice when compared to female wild-type mice (Figure 3.6 E). To determine the compositions of the K_{Ca} currents in aortic ECs, 200 nmol/L of Apa and 100 nmol/L of ChTX were applied one by one to the bath solution. The amount of the Apa-sensitive currents and the amount of the ChTX-sensitive currents were presented as the percentage of the total K_{Ca} currents in wild-type mice and $K_{Ca}3.1^{-/-}$ mice (Figure 3.6 F, G).

Patch-clamp experiments were also applied to investigate whether or not the inactivation of $K_{Ca}3.1$ channel altered other K_{Ca} channel current, i.e. $K_{Ca}2.3$ in aortic ECs of $K_{Ca}3.1^{-/-}$ mice. For this purpose, apamin-sensitive currents between $K_{Ca}3.1^{-/-}$ mice and their wild-type counterparts were compared. The apamin-sensitive K_{Ca} currents determined at 0 mV of membrane potential

were similar in ECs from $K_{Ca}3.1^{-/-}$ and wild-type mice of both sexes as shown in Figure 3.7.

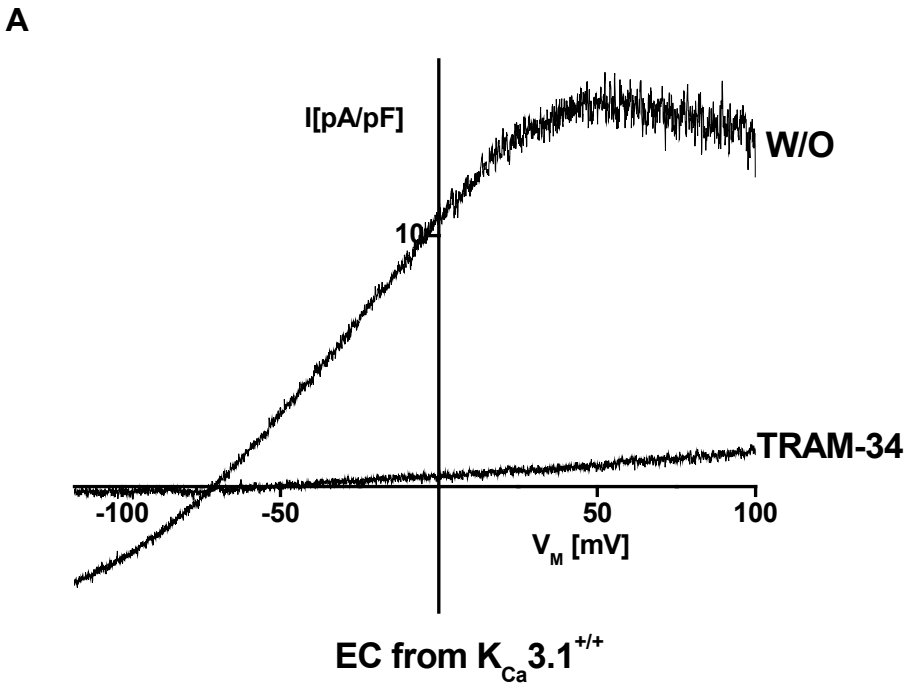
A
I[pA/pF]
10
W/O
TRAM-34
-100
-50
50
100
V_M [mV]
EC from K_Ca3.1^+/+

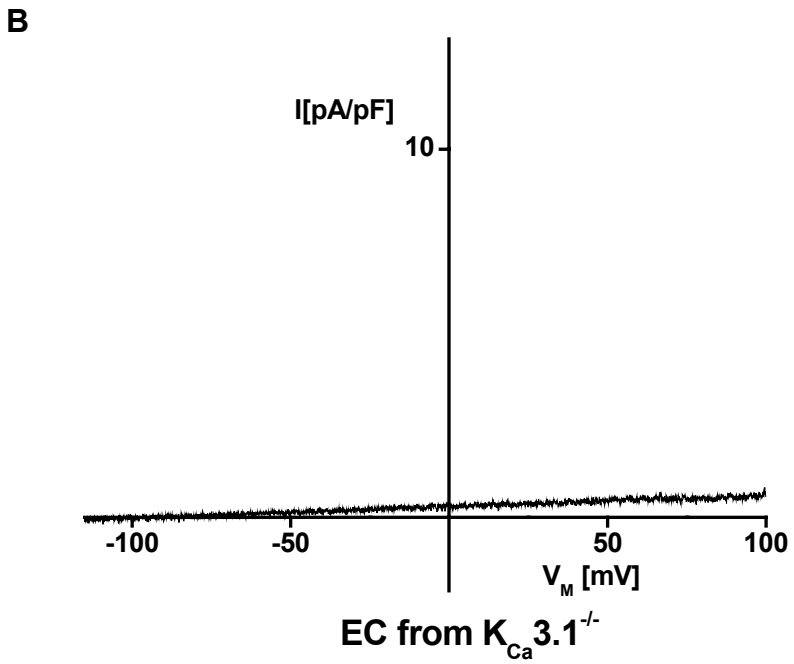
B
I[pA/pF]
10
-100
-50
50
100
V_M [mV]
EC from K_Ca3.1^-/-

C

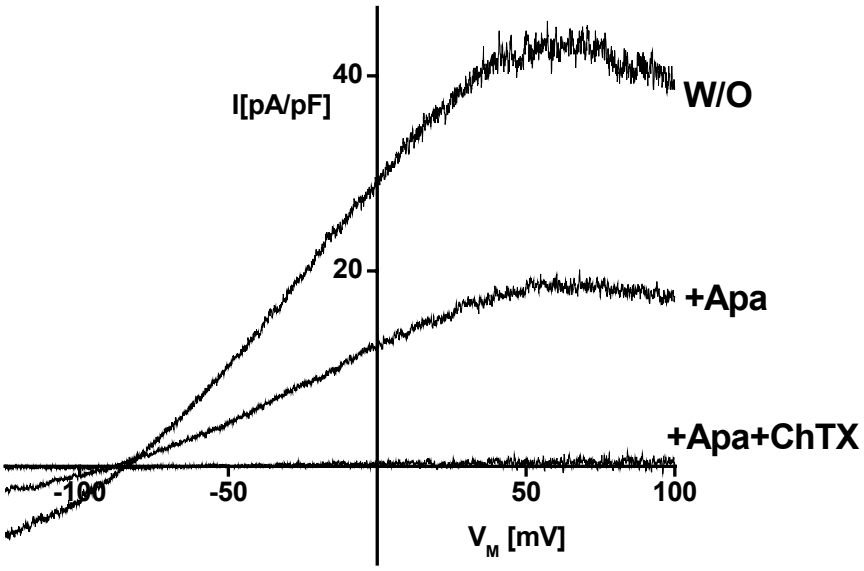

EC from $K_{Ca}3.1^{+/+}$

D

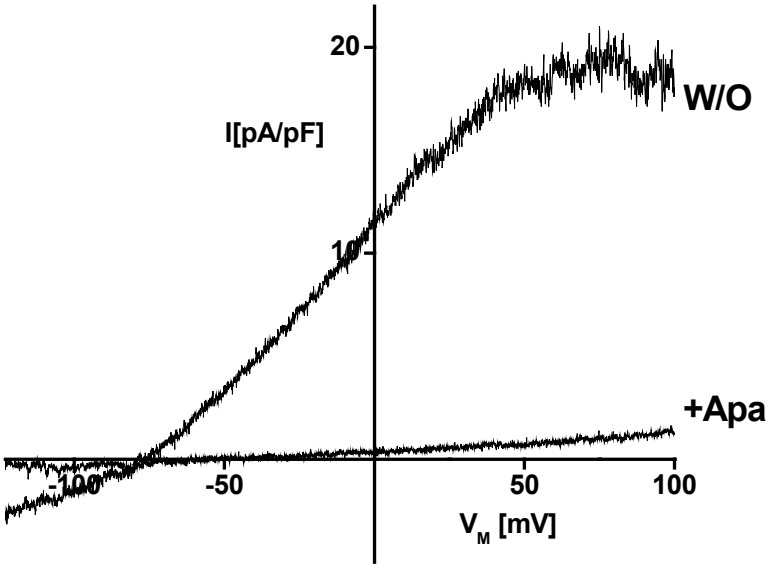

EC from $K_{Ca}3.1^{-/-}$

E

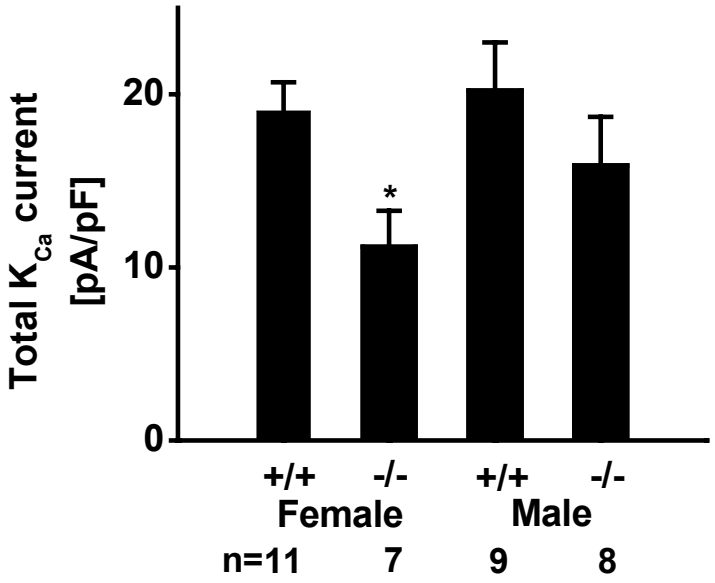
Total K_{Ca} current [pA/pF]
20
10
0
*
+/+
-/-
+/+
-/-
Female
Male
n=11
7
9
8

F

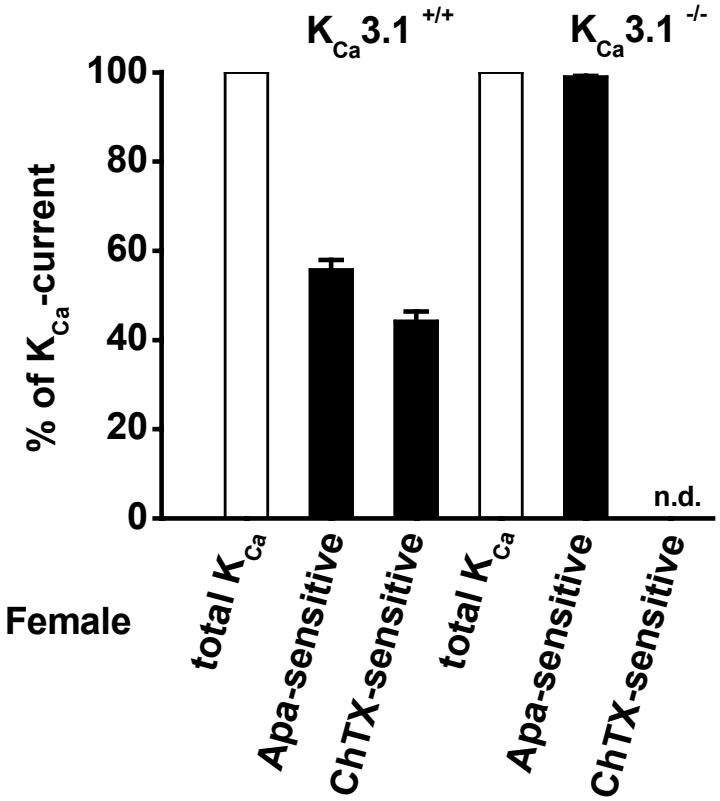
$K_{Ca}3.1^{+/+}$
$K_{Ca}3.1^{-/-}$
% of K_{Ca}-current
100
80
60
40
20
0
n.d.
Female
total K_{Ca}
Apa-sensitive
ChTX-sensitive
total K_{Ca}
Apa-sensitive
ChTX-sensitive

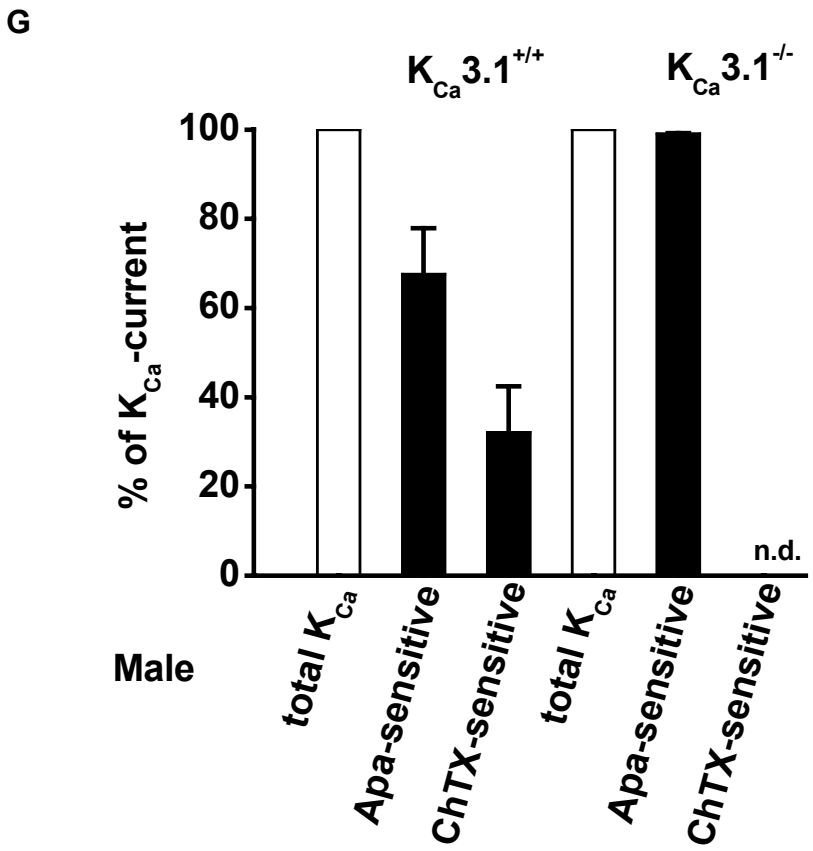

Figure 3.6 Characterization of the K_{Ca} currents in freshly isolated aortic ECs from $K_{Ca}3.1^{+/+}$ and $K_{Ca}3.1^{-/-}$ mice. **A**. Representative whole-cell currents recorded in ECs of $K_{Ca}3.1^{+/+}$ mice after dialysis with 3 µmol/L Ca^{2+} in the presence of 100 nmol/L of UCL1684 (w/o) in the bath. K_{Ca} currents were abolished by 0.2 µmol/L of TRAM-34. **B**. Representative traces recorded in ECs of $K_{Ca}3.1^{-/-}$ mice after dialysis with 3 µmol/L Ca^{2+} in the presence of 100 nmol/L of UCL1684 in the bath. **C**. Representative whole-cell currents recorded from $K_{Ca}3.1^{+/+}$ mice ECs after dialysis with 3 µmol/L Ca^{2+} (w/o) and inhibition of K_{Ca} currents by 100 nmol/L apamin and 100 nmol/L ChTX. **D**. Representative whole-cell currents recorded from $K_{Ca}3.1^{-/-}$ mice ECs after dialysis with 3 µmol/L Ca^{2+} (w/o) and inhibition of K_{Ca} currents by 100 nmol/L apamin. **E**. Comparisons of total K_{Ca} currents between $K_{Ca}3.1^{+/+}$ and $K_{Ca}3.1^{-/-}$ mice. +/+ represents $K_{Ca}3.1^{+/+}$ mice, -/-, $K_{Ca}3.1^{-/-}$ mice. **F**. The K_{Ca} currents from female mice ECs comprised of 55% (n=4) of Apa-sensitive currents and 44% (n=4) of ChTX-sensitive currents in wild-type and 99% of Apa-sensitive currents in $K_{Ca}3.1^{-/-}$ mice. **G**. The Ca^{2+}-activated K^+ currents from male mice ECs comprised of 67% (n=5) of Apa-sensitive currents and 32% (n=5) of ChTX-sensitive currents in wild-type and 99% of Apa-sensitive currents in $K_{Ca}3.1^{-/-}$ mice. ChTX-sensitive currents in female and male $K_{Ca}3.1^{-/-}$ mice are both not detectable (n.d.). Apa, apamin; ChTX, charybdotoxin. *P<0.05.

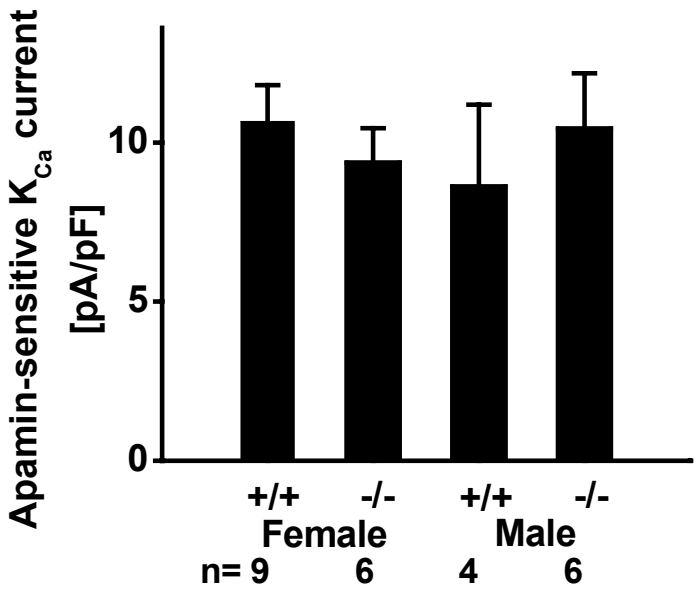

Figure 3.7 Comparisons of the apamin-sensitive K_{Ca} currents between ECs from $K_{Ca}3.1^{+/+}$ and $K_{Ca}3.1^{-/-}$ mice of both sexes. $K_{Ca}2.3$-currents were not statistically different between groups. Note that the apamin-sensitive K_{Ca} currents in ECs of male $K_{Ca}3.1^{-/-}$ mice showed a tendency to be increased when compared to the currents in ECs of male wild-type mice. +/+ represents $K_{Ca}3.1^{+/+}$ mice, -/-, $K_{Ca}3.1^{-/-}$ mice.

3.3.2 Ca^{2+} sensitivity of K_{Ca} current in female mice

To further investigate the sensitivity of K_{Ca} currents in $K_{Ca}3.1^{-/-}$ and wild-type mice, current densities were determined by dialysis with different cytosolic $[Ca^{2+}]_i$ and were compared between female $K_{Ca}3.1^{-/-}$ mice and their wild-type littermates.

Representative traces of K_{Ca} currents recorded in ECs dialyzed with 0.1, 0.3, 3.0 µmol/L of Ca^{2+}, respectively, were presented in Figure 3.8 A. K_{Ca} current densities were determined at 0 mV of membrane potential and subsequently mean current densities at different Ca^{2+} concentration were fitted to the

Boltzmann equation (see method part) to calculate the median effective concentration (EC_{50}) of cytosolic free Ca^{2+} (Figure 3.8). Thus, EC_{50}s of cytosolic $[Ca^{2+}]_i$ derived from Boltzmann equation were 343±17 nmol/L in female wild-type mice and 437±5 nmol/L in female $K_{Ca}3.1^{-/-}$ mice.

3.4 EDHF-mediated vasodilation in $K_{Ca}3.1$ transgenic mice

To investigate and compare the EDHF-mediated vasodilation between $K_{Ca}3.1^{-/-}$ mice and $K_{Ca}3.1^{+/+}$ mice, pressure myograph experiments were performed using freshly isolated carotid arteries (CA).

For induction of EDHF-mediated vasodilation, acetylcholine (ACh) was applied to the lumen of phenylephrine-preconstricted CAs from $K_{Ca}3.1^{-/-}$ and wild-type mice. ACh induced a dose-dependent NO-and PGI_2-resistant EDHF-type vasodilation (Figure 3.9 A&B).

At all concentrations of ACh when considerable vasodilation was induced (≥ 100 nmol/L), EDHF-mediated vasodilatory responses were significantly decreased in CAs of female $K_{Ca}3.1^{-/-}$ mice when compared to wild-type female mice (Figure 3.9 A). At a physiologically relevant concentration of ACh (100 nmol/L), EDHF-mediated vasodilation was reduced by ≈50% in female $K_{Ca}3.1^{-/-}$ mice when compared to wild-type littermates. In addition, EDHF-mediated vasodilation also showed a significant reduction in the maximal response to 10 µmol/L of ACh in female $K_{Ca}3.1^{-/-}$ mice when compared to their wild-type littermates. On the contrary, ACh-induced EDHF-type vasodilation only showed a tendency to be decreased in $K_{Ca}3.1^{-/-}$ male mice without statistical significance when compared to $K_{Ca}3.1^{+/+}$ male mice (Figure 3.9 B).

Intraluminal application of the selective $K_{Ca}3.1$ and $K_{Ca}2.3$ opener DC-EBIO (10 µmol/L)-induced vasodilation was also significantly reduced by ≈20% in CAs of female $K_{Ca}3.1^{-/-}$ mice when compared to their wild-type littermates (Figure 3.9 C), while in CAs of male $K_{Ca}3.1^{-/-}$ mice there was no significant change (Figure 3.9 D).

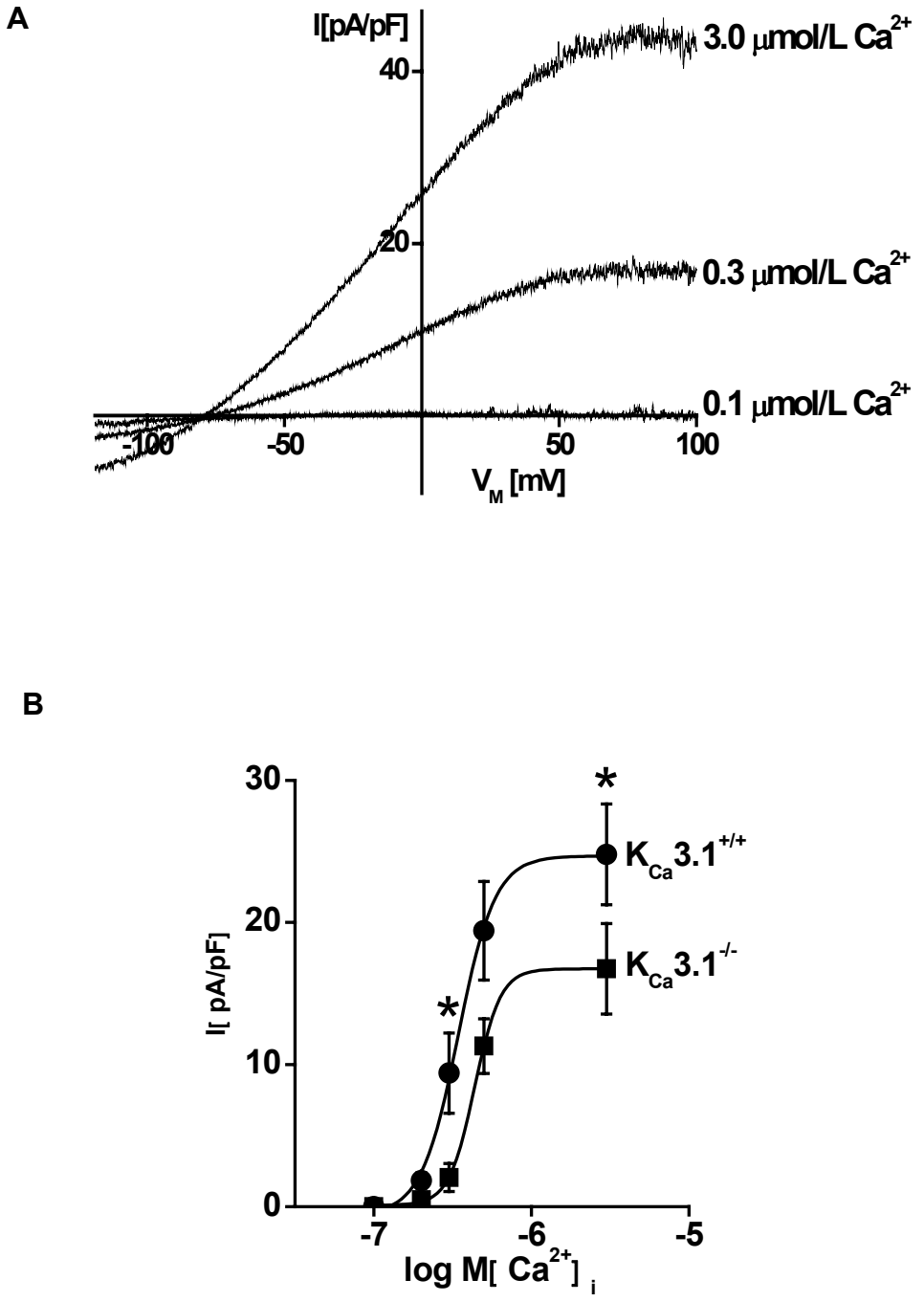

Figure 3.8 Ca^{2+}-sensitivity of K_{Ca} currents in aortic ECs of female mice. **A**. Representative traces of K_{Ca} currents recorded in ECs of female $K_{Ca}3.1^{+/+}$ mice dialyzed with 0.1, 0.3, 3.0 µmol/L of Ca^{2+}, respectively. **B**. Current densities were measured using 0.1 (n=5), 0.2 (n=5), 0.3 (n=5), 0.5 (n=6), 3.0 (n=8) µmol/L cytosolic $[Ca^{2+}]_i$ Data were showed as mean±SE and fitted to the Boltzmann equation. **P*<0.05.

A

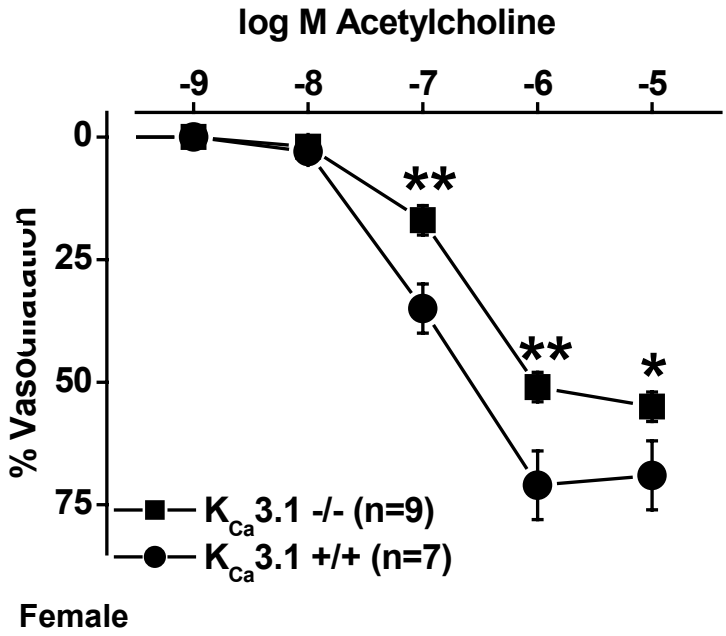

Female

B

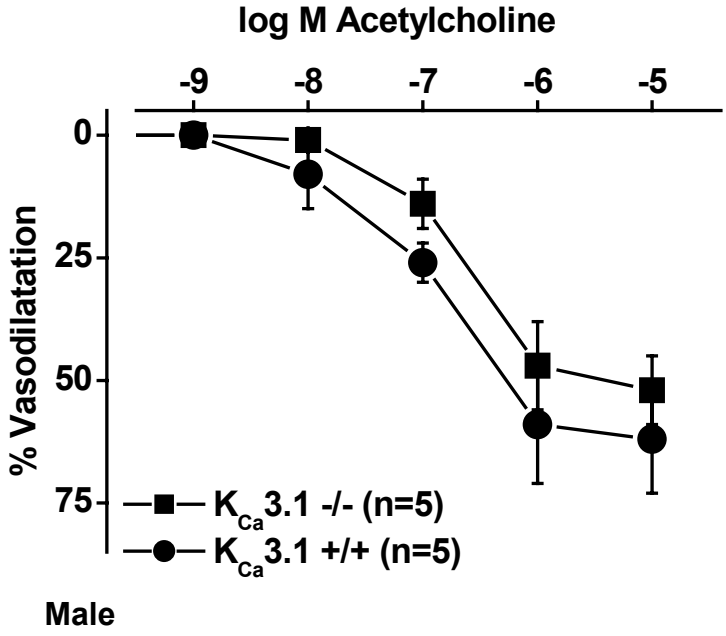

Male

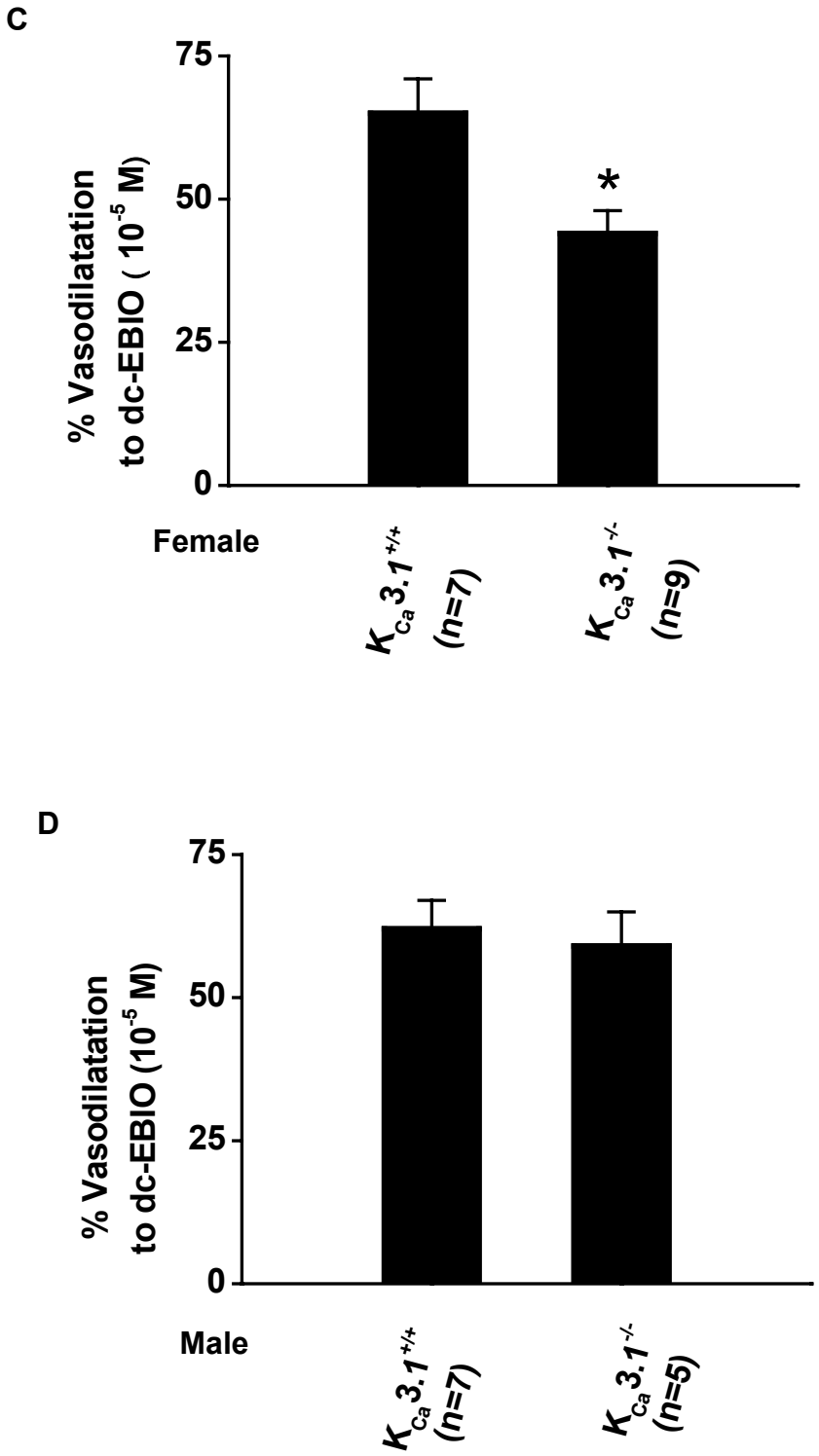

Figure 3.9 EDHF-mediated vasodilation in $K_{Ca}3.1^{+/+}$ and $K_{Ca}3.1^{-/-}$ mice. **A**. Dose-dependent vasodilation in response to intraluminal application of ACh in CAs of $K_{Ca}3.1^{+/+}$ female mice and $K_{Ca}3.1^{-/-}$ female mice. **B**. Dose-dependent vasodilation in response to intraluminal application of ACh in CAs of $K_{Ca}3.1^{+/+}$ male mice and $K_{Ca}3.1^{-/-}$ male mice. **C**. Vasodilation in response to intraluminal application of 10 µmol/L DC-EBIO in $K_{Ca}3.1^{+/+}$ female mice and $K_{Ca}3.1^{-/-}$ female mice CAs. **D**. Vasodilation in response to intraluminal application of 10 µmol/L DC-EBIO in $K_{Ca}3.1^{+/+}$ male mice and $K_{Ca}3.1^{-/-}$ male mice CAs. *P<0.05; **P<0.01. Data (percentage of maximal dilation) are given as mean±SE.

3.5 Inactivation of $K_{Ca}3.1$ increases systemic blood pressure

Because the inactivation of $K_{Ca}3.1$ channel in female mice greatly reduced the EDHF-mediated vasodilation of CA, it was hypothesized that this may result in an increased systemic blood pressure in female mice. To measure the mice blood pressure, the non-invasive tail-cuff experiments were performed first. Data are summarized in Figure 3.10. While quiescent female $K_{Ca}3.1^{+/+}$ mice showed a normal systolic blood pressure (SBP) of about 127 mmHg, female $K_{Ca}3.1^{-/-}$ mice had an elevated SBP of about 139 mmHg (Figure 3.10 A). The same tail-cuff experiments were also performed in male mice, but the SBP was not significantly different in $K_{Ca}3.1^{-/-}$ male mice when compared to their wild-type littermates (Figure 3.10 B).

To confirm the influence of the lack of $K_{Ca}3.1$ on the systemic blood pressure as deduced from tail-cuff measurements, telemetry was performed in a smaller set of female mice. Data showed an about 11 mmHg elevated SBP in female $K_{Ca}3.1^{-/-}$ mice when compared to the wild-type female mice (Figure 3.11). The diastolic blood pressures (DBP) in female $K_{Ca}3.1^{-/-}$ mice tended to increase when compared to their wild-type littermates though the difference did not reach statistical significance. The calculated mean arterial pressure (MAP) was also significantly increased by about 8 mmHg in female $K_{Ca}3.1^{-/-}$ mice when compared to the female $K_{Ca}3.1^{+/+}$ mice (Figure 3.11).

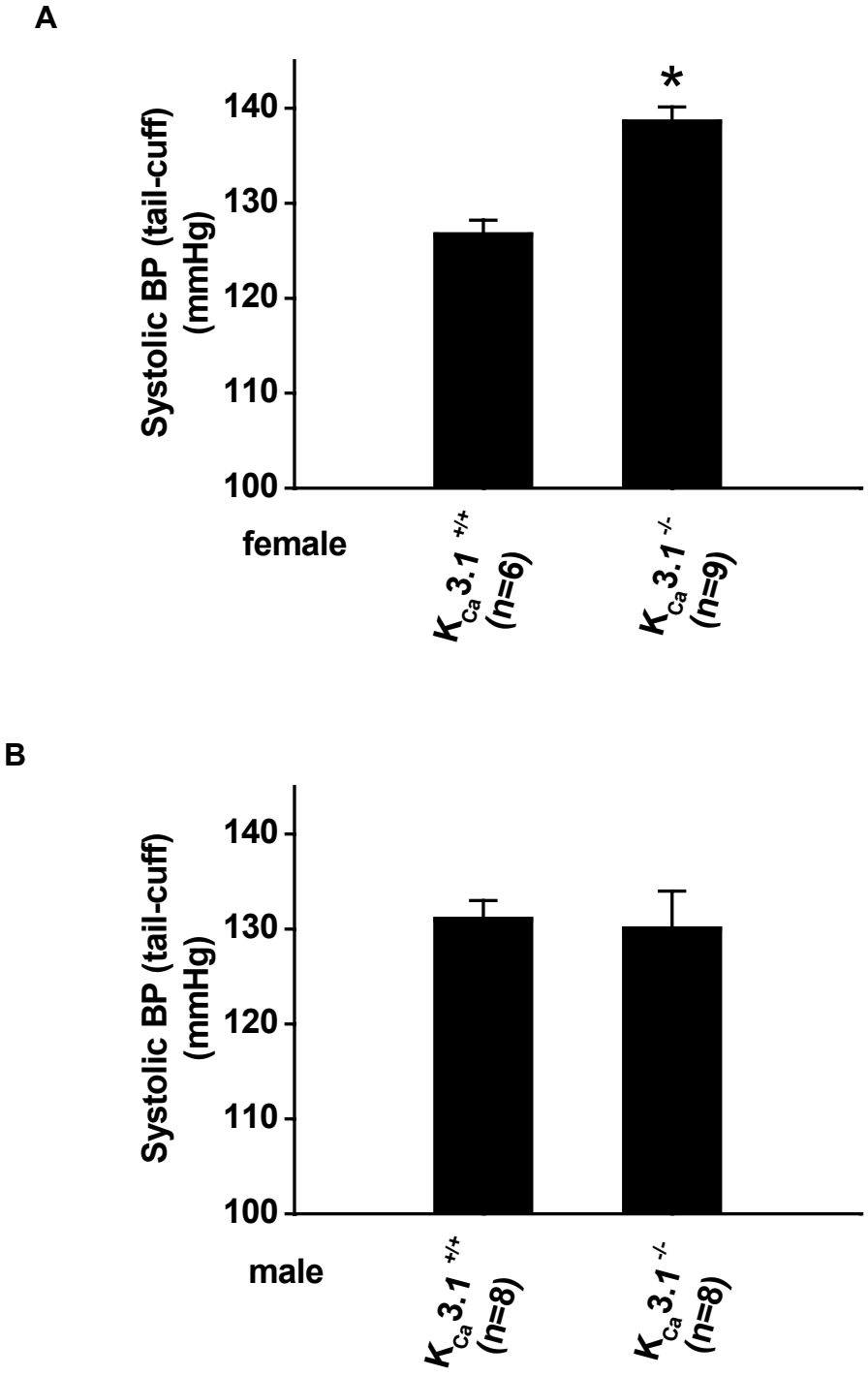

Figure 3.10 Systolic blood pressures (SBP) of female (A) and male (B) mice measured by non-invasive tail-cuff experiments. *P<0.05.

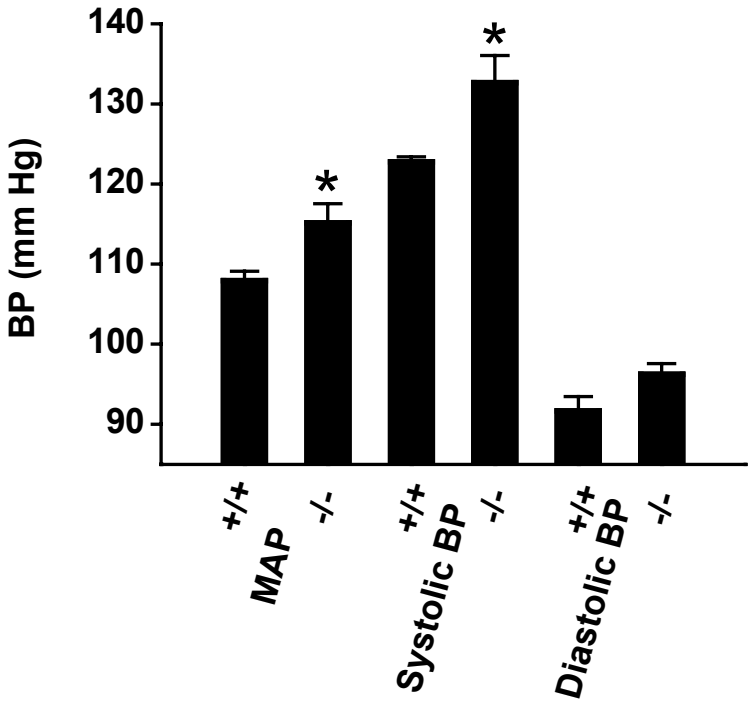

Figure 3.11 Telemetry blood pressure studies of female mice. Systolic blood pressure (SBP), diastolic blood pressure (DBP) were measured (n=4), mean arterial pressure (MAP) was calculated using MAP=DBP+1/3(SBP-DBP). +/+ represents female $K_{Ca}3.1^{+/+}$ mice; -/-, female $K_{Ca}3.1^{-/-}$ mice. **P*<0.05.